

1 **Air temperature variability over three glaciers in the Ortles-Cevedale (Italian**
2 **Alps): effects of glacier fragmentation, comparison of calculation methods and**
3 **impacts on mass balance modeling**

4
5 Luca Carturan¹, Federico Cazorzi², Fabrizio De Blasi¹, Giancarlo Dalla Fontana¹

6 ¹ Department of Land, Environment, Agriculture and Forestry, University of Padova, Viale
7 dell'Università 16 - 35020 - Legnaro, Padova, Italy

8 ² Department of Agriculture and Environmental Sciences, University of Udine, via delle Scienze
9 208 - 33100 - Udine, Italy

10
11 Corresponding author: luca.carturan@unipd.it
12

13
14 **Abstract**

15 Glacier mass balance models rely on accurate spatial calculation of input data, in particular air
16 temperature. Lower temperatures (the so-called glacier cooling effect), and lower temperature
17 variability (the so-called glacier damping effect) generally occur over glaciers, compared to ambient
18 conditions. These effects, which depend on the geometric characteristics of glaciers and display a
19 high spatial and temporal variability, have been mostly investigated on medium- to large-size
20 glaciers so far, while observations on smaller ice bodies ($< 0.5 \text{ km}^2$) are scarce. Using a dataset
21 from 8 on-glacier and 4 off-glacier weather stations, collected in summer 2010 and 2011, we
22 analyzed the air temperature variability and wind regime over three different glaciers in the Ortles-
23 Cevedale. The magnitude of the cooling effect and the occurrence of katabatic boundary layer
24 (KBL) processes showed remarkable differences among the three ice bodies, suggesting the likely
25 existence of important reinforcing mechanisms during glacier decay and fragmentation. The
26 methods proposed by Greuell and Böhm (1998) and Shea and Moore (2010) for calculating on-
27 glacier temperature from off-glacier data did not fully reproduce our observations. Among them, the
28 more physically-based procedure of Greuell and Böhm (1998) provided the best overall results
29 where the KBL prevails, but it was not effective elsewhere (i.e. on smaller ice bodies and close to
30 the glacier margins). The accuracy of air temperature estimations strongly impacted the results from
31 a mass balance model which was applied to the three investigated glaciers. Most importantly, even
32 small temperature deviations caused distortions in parameter calibration, thus compromising the
33 model generalizability.

34 **1 Introduction and background**

35 Air temperature exerts a crucial control on the energy and mass exchanges occurring at the glacier
36 surface. It regulates the accumulation processes via the snowfall elevation limit and the snowpack
37 metamorphism (which affect redistribution phenomena), and regulates the ablation processes via
38 turbulent fluxes and longwave radiation. It is also closely related to important feedbacks such as
39 albedo, the mass balance–elevation feedback, and the glacier cooling effect, which changes as
40 glaciers adjust their size in response to climatic fluctuations (Khodakov, 1975; Klok and Oerlemans,
41 2004; Paul et al., 2005; Raymond and Neumann, 2005; Haeberli et al., 2007; Fischer, 2010; Paul,
42 2010; Carturan et al., 2013).

43 Distributed models of different complexity have been proposed for calculating the mass balance of
44 glaciers under different climatic scenarios at a variety of spatial scales and with different purposes.
45 The current concern about sea level rise and future availability of water resources stored in glaciers,
46 under projected global warming scenarios, has led to increased efforts to develop models able to
47 account for i) direct effects of climate change, and ii) reinforcing mechanisms which control glacier
48 decay (Hock, 2005; Barry, 2006).

49 These models rely on accurate spatial calculation of input data, in particular air temperature, which
50 affects not only their final performance but also the calibration of parameters and model
51 generalizability. Indeed, wrong temperature estimates lead to wrong calibration and/or distortion of
52 parameters, possibly hampering the applicability of models to ungauged catchments, despite the
53 good knowledge achieved for individual processes (Savenije, 2001; Sivapalan, 2006).

54 Charbonneau et al. (1981), for example, highlighted that issues in extrapolating meteorological
55 input data are much more crucial than the possible choice between different approaches for
56 modeling snow yields from a well-equipped catchment in the French Alps. Similarly,
57 intercomparison projects of runoff models by the World Meteorological Organization (e.g. WMO,
58 1986) revealed that simple models provided comparable results to more sophisticated models, given
59 the difficulties of assigning proper model parameters and meteorological input data to each
60 catchment element. Machguth et al. (2008), analyzing model uncertainty with Monte Carlo
61 simulations at one point on the tongue of Morteratsch Glacier in Switzerland, concluded that the
62 output of well-calibrated models, when applied to extrapolate in time and space, is subject to
63 considerable uncertainties due to the quality of input data. According to Carturan et al. (2012a),
64 who compared three melt algorithms in a six-year application of an enhanced temperature-index
65 model over two Italian glaciers, uncertainties in extrapolating temperature measurements from off-
66 site data partly mask the peculiar behavior of each algorithm and do not allow definitive
67 conclusions to be drawn.

68 Two main issues affect the correct estimation of air temperature distribution over glacial surfaces: i)
69 the absence of on-site weather stations in most operational model applications, and ii) the
70 development of a katabatic boundary layer (KBL) over the typically inclined glacier surfaces (van
71 den Broeke, 1997). Several experiments with automatic weather stations deployed over glaciers
72 demonstrated that general assumptions in extrapolating air temperature, based on the application of
73 fixed lapse rates which account for the linear dependency of ambient (i.e. off-glacier) temperature
74 on altitude, have serious limitations (e.g. Greuell et al., 1997; Strasser et al., 2004; Petersen and
75 Pellicciotti, 2011).

76 In particular, these assumptions do not apply when katabatic flows and the KBL form, that is,
77 during the ablation season on melting mid-latitude glacial surfaces, when the ambient temperature is
78 higher than the surface temperature which cannot exceed 0°C. Katabatic winds are gravity winds
79 originated by the cooling of the near-surface air layers, resulting in density gradients which force a
80 downward movement of the air under the effect of gravity. The two main processes affecting the

81 temperature of the air during this downslope movement are the cooling due to the exchange of
82 sensible heat and the adiabatic heating. The interplay of these processes has a twofold effect,
83 consisting in lower on-glacier temperatures (the so-called glacier cooling effect), and lower
84 temperature variability (the so-called glacier damping effect, also referred to as reduced climate
85 sensitivity), compared to ambient conditions (Braithwaite, 1980; Greuell and Böhm, 1998;
86 Braithwaite et al., 2002; Gardner et al., 2009). As a result, on-glacier lapse rates generally differ
87 from average environmental lapse rates (i.e. $-0.0065^{\circ}\text{C m}^{-1}$). Cooling and damping effects are not
88 homogeneous over glacial surfaces, and mainly depend on the size and geometric characteristics, in
89 particular the slope, of single glaciers, and on the specific position along the glacier. Generally, they
90 are directly related to the size of glaciers and the fetch distance along the flowline, and inversely
91 related to the slope of glaciers. The latest controls the prevalence of the cooling due to turbulent
92 exchanges over the adiabatic heating of air forced to move downward by katabatic winds.

93 Few methods have been proposed in the literature to model these processes, mainly due to the
94 scarcity of glaciers instrumented for distributed measurements of air temperature. Among the first
95 authors who measured the glacier cooling effect, defined as the temperature difference between an
96 on-glacier and an off-glacier site with the same altitude, we can cite Schytt (1955) and Eriksson
97 (1958), who detected temperature depressions ranging from 1.1 to 2.2°C on Storglaciären (Sweden)
98 and 3 to 4°C on Skagastøl Glacier (Norway), respectively. Havens (1964) measured an average
99 cooling effect ranging from 1.5°C to 2.7°C at a weather station located 1 km up-glacier from the
100 terminus of White Glacier (Canada), recognizing maximum values during warm and sunny weather
101 and minimum values during overcast and unsettled weather.

102 To our knowledge, the first attempt to parameterize the mean summer cooling effect at the firn line
103 altitude was made by Khodakov (1975), who proposed a relationship with glacier length, based on
104 temperature data obtained from mountain glaciers and ice sheets. Analyzing direct observations
105 from glaciers in Caucasus, Pamir, Scandinavia, Thien Shan, and Altay, Davidovich and Ananicheva
106 (1996) provided a simple relationship for calculating the mean summer temperature at the
107 equilibrium line altitude (ELA) in function of the mean off-glacier summer temperature at the same
108 altitude. The same authors suggested that the cooling effect is maximal at the ELA and decreases
109 towards both the terminus and up-glacier.

110 The first comprehensive glacio-meteorological experiment providing distributed temperature
111 measurements was carried out in summer 1994 on Pasterze Glacier, Austria, and comprised five
112 automatic weather stations (AWS) placed along a flowline. From this experiment, Greuell and
113 Böhm (1998) developed a thermodynamic model for calculating air temperature in function of slope
114 and distance along the flowline, accounting for sensible heat exchanges and adiabatic heating.
115 Braithwaite et al. (2002) used an empirical approach and a formulation derived from data gathered
116 in two Canadian Arctic glaciers (Sverdrup and White), similar to that proposed by Davidovich and
117 Ananicheva (1996) but applied to monthly temperatures. Shea and Moore (2010) suggested
118 empirical relationships based on piecewise linear regressions of on-glacier versus ambient
119 temperatures collected in British Columbia (Canada) between 2006 and 2008, for calculating i) the
120 threshold temperature triggering KBL development, and ii) the glacier damping effect, as a function
121 of elevation and flow path length (i.e. the ‘average flow distance to a given point starting from an
122 upslope limit or ridge’).

123 At present these methods have rarely been used by other authors, and they have not been compared
124 using independent test sites. Petersen et al. (2013) tested the Greuell and Böhm (1998) model using
125 a dataset of air temperature measurements from Haut Glacier d'Arolla, Switzerland, concluding that
126 results of spatial extrapolations along the glacier are only a little better than using a constant linear
127 lapse rate calculated between on-glacier data points, attributing this result to the spatial variability
128 of the thickness of the glacier boundary layer.

129 The transferability of the proposed methods remains to be tested. In addition, it should be noted that
130 many of them have been developed using temperature data collected from medium- (from 0.5 to 10
131 km²) to large-sized (larger than 10 km²) glaciers. As the glacier cooling effect and the damping
132 effect depend on the size of glaciers, it is opportune to investigate the thermal effects of ice bodies
133 smaller than 0.5 km², which are widespread and increasing in number in mid-latitude mountain
134 regions as a result of rapid shrinking and fragmentation.

135 In this work we present the results of a glacio-meteorological experiment, carried out in summer
136 2010 and 2011, deploying several automatic weather stations over three neighboring glaciers in the
137 Ortles-Cevedale mountain group (Italian Alps). The study was focused on the variability of air
138 temperature over the three glaciers, which differ in size, geometric characteristics, and reaction to
139 climatic changes (Carturan et al., 2014). In this paper, we analyze the temporal and spatial behavior
140 of air temperature and glacier cooling effect in the study area, testing existing methods for
141 calculating on-glacier temperatures from off-site data, and evaluating their impact in mass balance
142 simulations using a distributed enhanced temperature-index (ETI) model.

143

144 **2 Study area**

145 The investigated glaciers are located in the Alta Val de la Mare (AVDM), Eastern Italian Alps (Fig.
146 1). This 36 km² experimental watershed is the subject of detailed studies concerning the impacts of
147 climate change on the cryosphere and hydrology. The area has previously been selected for
148 studying the behavior of meteorological variables at high altitude (Carturan et al., 2012b) and for
149 developing an enhanced temperature-index glacier mass balance model (Carturan et al., 2012a). The
150 highest summit is Mt Cevedale (3769 m a.s.l.), while the basin outlet is located at 1950 m a.s.l. The
151 catchment lies in the southern part of the Ortles-Cevedale massif, the largest glacierized mountain
152 group in the Italian Alps. The Careser diga weather station (2607 m a.s.l.) has been operating since
153 the 1930s, recording daily 2 m air temperature, precipitation, snow depth, and fresh-snow height. In
154 the 1990s, an automatic weather station replaced the old manual instruments. At this site, the mean
155 1979–2009 annual precipitation (corrected for gauge errors) was 1233 mm and the mean annual air
156 temperature in the same period was –0.5 °C.

157 The investigated glaciers are very different. Careser Glacier (2870– 3279 m a.s.l.) is flat and mainly
158 exposed to the south. In 2005 it spread in two parts: Careser Orientale (2.13 km² in 2006) and
159 Careser Occidentale (0.27 km² in 2006). La Mare Glacier (2650–3769 m a.s.l., 3.79 km² in 2006)
160 faces to the east and is steeper. On all glaciers, topographic shading is of minor importance. The
161 Careser glaciers have no accumulation area and exhibit down-wasting and fragmentation in smaller
162 units (Carturan et al., 2013), while La Mare Glacier still has an accumulation area and shows ‘active’
163 retreat towards higher altitudes (Zanon, 1982; Small, 1995; Carturan et al., 2009 and 2014). Long-
164 term monitoring programs started in 1967 on Careser and in 2003 on La Mare. In the last 10 years,
165 the glaciers have been the subject of investigations on snow accumulation, snow and ice ablation,
166 point energy balance, and runoff generation (Carturan, 2010).

167

168 **3 Methods**

169 **3.1 Experimental setup**

170 An automatic weather station (AWS) has been operating since July 2007 on the ablation area of La
171 Mare Glacier (2973 m a.s.l.), measuring air temperature and relative humidity, wind speed and
172 direction, incoming and outgoing shortwave and longwave radiation, and snow depth. The thermo-

173 hygrometric probe is housed in a ventilated radiation shield. Data are sampled every 60 seconds,
174 with 15 minute means being stored in a Campbell Scientific CR1000 datalogger; the AWS is
175 powered by a 25 W solar panel. Data were periodically downloaded with a portable laptop until
176 July 2011. Since August 2011, a satellite modem has automatically transmitted data at three-day
177 intervals (Abbate et al., 2013).

178 On 3 July 2010 three Vantage Pro Plus (VPP) weather stations, manufactured by Davis Instruments,
179 were placed along a longitudinal profile on La Mare Glacier at elevations ranging from 2709 m,
180 close to the terminus, to 3438 m, near to the upper divide. Davis VPP stations are low-cost,
181 commercial weather stations, characterized by a compact design and low weight, and can be moved
182 rather easily along glaciers by few persons. Their thermo-hygrometric probe is shielded by a
183 ventilated screen, which is important for air temperature measurements in high-radiation and/or
184 low-wind speed conditions on glaciers (Georges and Kaser, 2002). Hourly mean data are stored in a
185 Davis datalogger. During the experiment, the data were downloaded with a portable laptop every
186 two weeks. The three VPP were removed on 23 September 2010.

187 On 7 July 2011 four VPP stations were deployed, two on Careser Glacier and two on La Mare
188 Glacier. One weather station was re-positioned at 3438 m on La Mare Glacier because
189 instrumentation failure occurred at that place in 2010, due to lightning damage. The other three
190 weather stations were placed in areas where systematic errors in mass balance simulations were
191 recognized by Carturan et al. (2012a), who applied a mass balance model using the standard
192 environmental lapse rate for extrapolating air temperature from an off-glacier weather station, as
193 commonly used in most model applications where on-glacier data are not available. The four VPP
194 were removed on 12 September 2011.

195 Table 1 reports the configuration of the weather stations operated on Careser and La Mare glaciers,
196 whose location is shown in Fig. 1. Four off-glacier weather stations (Table 1) were also used in this
197 study for the calculation of the glacier cooling effect in comparison to ambient temperature, and for
198 testing two methods of calculation of on-glacier temperatures from off-site data. Two of them are
199 part of the regional weather station networks (Bel_3328, at Cima Beltovo, 3328 m a.s.l.; Cog_1202,
200 at Cogolo Pont, 1202 m a.s.l., Fig. 1). The other two weather stations consist of Hobo Pro
201 dataloggers (Onset Computer Corporation) installed at Careser diga (Car_2607, at 2607 m a.s.l.)
202 and close to Careser Glacier (Car_3051, at 3051 m a.s.l.). All these stations are far enough from the
203 thermal influence of glaciers (minimum distance of 300 m from Car_3051 to the margin of Careser
204 Glacier), and equipped with temperature probes housed in naturally ventilated radiation shields.
205 Possible issues related to the use of different types of temperature sensors and radiation shields are
206 addressed in the following section.

207 **3.2 Data processing and accuracy assessment**

208 For our analyses, hourly means were calculated from sub-hourly meteorological data. After being
209 synchronized with local solar time, the data were checked for possible gaps, outliers, and
210 inhomogeneities. The major gap concerned a few days in summer 2011 for the precipitation data at
211 Careser diga, which were filled using the manual observations recorded by the personnel of the
212 local hydropower company. Other gaps of 1-2 hours occurred during the maintenance of weather
213 stations, and were filled by linear interpolation.

214 The spatial density and type of weather stations used in this study were decided based on i) the pre-
215 existing network of regional AWSs and ii) the logistic constraints affecting the access to the
216 glaciers and limiting the number of research-grade AWSs which could be deployed. These
217 limitations are common in mountain regions, and imposed comparable or even lower densities of
218 AWSs, as well as the use of different types of sensors with different radiation shields, in most

219 similar studies on glaciers (e.g. Shea and Moore, 2010; Petersen and Pellicciotti, 2011; Petersen et
220 al., 2013).

221 Intercomparison tests have been carried out in order to assess the impact of using different sensors
222 and radiation shields for this study. The four VPP weather stations were run for some days within a
223 10-m radius, both before and after the glacio-meteorological experiment, confirming the almost
224 identical readings of air temperature, wind speed, and wind direction. Mean differences in air
225 temperature data during the tests were lower than 0.20°C (maximum STD = 0.16°C). For
226 comparison purposes, one VPP was run close to the AWS of La Mare Glacier in summer 2009,
227 revealing mean differences in air temperature readings of 0.10°C (STD = 0.12°C). A further
228 comparison was carried out in the summers of 2007 and 2008, running a VPP close to the Hobo Pro
229 datalogger and close to a temperature sensor of the regional weather service installed at Careser
230 diga. These two instruments, which have natural ventilation systems, showed mean differences of
231 0.10°C (STD = 0.40°C) and 0.23°C (STD = 0.66°C), respectively, compared to the aspirated VPP.
232 Based on these results, no corrections were applied to the measured air temperatures.

233 3.3 Analysis of field data

234 The meteorological data collected by the weather stations were firstly analyzed calculating
235 descriptive statistics for each of the two summers 2010 and 2011 and focusing on vertical lapse
236 rates. Afterwards, the data were analyzed at hourly resolution focusing on the calculation of
237 ambient (i.e. off-glacier) temperature, which is crucial for estimating on-glacier near-surface
238 temperatures, and is required by all methods proposed in the literature for this purpose. Moreover,
239 the correct estimation of the ambient temperature is an essential prerequisite for quantifying the
240 site-specific cooling effect on glaciers, which is defined as 'the difference between screen-level
241 temperatures over glaciers compared to equivalent-altitude temperatures in the free atmosphere'
242 (Braithwaite, 1980). Different combinations of lapse rates (i.e. fixed standard or hourly-variable
243 obtained by linear regression of temperature versus elevation) and subsets of weather stations were
244 tested (see details in Sect. 4.2).

245 The spatial and temporal variability of the cooling effect was then investigated, plotting the average
246 diurnal cycle of the cooling effect versus average cycles of wind speed and direction, and drawing
247 charts of the daily average cooling effect vs. daily temperature and precipitation recorded at Careser
248 diga, in order to assess the role of different weather types in the glacial temperature regimes.

249 3.4 Calculation of on-glacier temperature from off-site data

250 The measured on-glacier temperatures served for testing the procedures suggested by Shea and
251 Moore (2010) and Greuell and Böhm (1998) (from now on “S&M” and “G&B”, respectively) for
252 calculating the air temperature distribution over glacierized surfaces. The empirical methods by
253 Khodakov (1975), Davidovich and Ananicheva (1996), and Braithwaite et al. (2002) were not tested
254 because they are more empirical, the coefficients were calculated in very different environments,
255 and they do not take into account the temporal variability of the cooling effect.

256 S&M suggested the use of a piecewise regression model:

$$257 T_g(x, t) = \begin{cases} T_1 + k_2(T_a - T^*), & T_a \geq T^* \\ T_1 - k_1(T^* - T_a), & T_a < T^* \end{cases} \quad (1)$$

258 where $T_g(x, t)$ (°C) is the on-glacier temperature for site x at time t , T^* (°C) represents a threshold
259 ambient temperature for KBL effects on T_g , T_l (°C) is the corresponding on-glacier threshold
260 temperature, k_2 (k_l) is the so called sensitivity of on-glacier temperature to ambient temperature (T_a ,
261 °C) changes when T_a is above (below) T^* . Empirical transfer functions were obtained by S&M,

262 relating the fitted coefficients (T^* , k_1 and k_2) for each weather station used in their work to
 263 topographic attributes extracted from a digital elevation model (DEM):

$$264 \quad T^* = \beta_1 + \beta_2 Z \quad (2)$$

$$265 \quad k_1 = \beta_3 \exp(\beta_4 FPL) \quad (3)$$

$$266 \quad k_2 = \beta_5 + \beta_6 \exp(\beta_7 FPL) \quad (4)$$

267 where β_i are the coefficients of the transfer functions, Z (m) is the elevation, and FPL (m) is the
 268 flow path length, defined as ‘the average flow distance to a given point starting from an upslope
 269 summit or ridge’ (Shea and Moore, 2010). T_I is calculated as $T^* \cdot k_I$.

270 The G&B model assumes the presence of a katabatic wind, and therefore it applies when the
 271 ambient temperature is higher than the surface temperature. In these conditions the potential
 272 temperature θ ($^{\circ}\text{C}$) at the distance x along the flowline ($x = 0$ at the top of the flowline) is calculated
 273 as:

$$274 \quad \theta(x) = (T_0 - T_{eq}) \exp\left(-\frac{x-x_0}{L_R}\right) - b(x + x_0) + T_{eq} \quad (5)$$

275 with

$$276 \quad T_0 = T_{cs} - \gamma(z_{cs} - z_0) \quad (6)$$

$$277 \quad T_{eq} = bL_R \quad (7)$$

$$278 \quad L_R = \frac{H \cos(\alpha)}{C_H} \quad (8)$$

$$279 \quad b = \Gamma_d \tan(\alpha) \quad (9)$$

280 where T_0 ($^{\circ}\text{C}$) is the temperature at $x = 0$, T_{eq} ($^{\circ}\text{C}$) is defined as the ‘equilibrium temperature’, x_0
 281 and z_0 (m) are the location and elevation where the air enters the glacier-wind layer, T_{cs} ($^{\circ}\text{C}$) and z_{cs}
 282 (m) are the temperature and the elevation at the off-glacier weather station, γ ($^{\circ}\text{C m}^{-1}$) is the ambient
 283 lapse rate, H (m) is the height of the glacier wind layer, α ($^{\circ}$) is the glacier slope, C_H is the bulk
 284 transfer coefficient for heat, and Γ_d is the dry adiabatic lapse rate ($-0.0098^{\circ}\text{C m}^{-1}$). The potential
 285 temperature is converted into temperature by means of:

$$286 \quad T(x, z) = \theta(x) - \Gamma_d [z(x = 0) - z(x)] \quad (10)$$

287 where $z(x)$ is the surface profile of the glacier.

288 For both methods, the original formulations and parameters were tested unchanged against our
 289 experimental data, evaluating also possible modifications as detailed in Sect. 4. The efficiency was
 290 evaluated by means of three different statistics: i) the mean error (ME), ii) the root mean square
 291 error (RMSE), and iii) the efficiency criterion by Nash and Sutcliffe (N&S, 1970). The topographic
 292 information required to apply these methods was extracted from a 2 x 2 m DEM surveyed by
 293 LiDAR in late summer of 2006. A map of the FPL was calculated from this DEM, using algorithms
 294 developed for drainage area calculations (Fig. 2, Tarboton et al., 1991).

295 **3.5 Mass balance modeling**

296 The impact that the calculation of on-glacier temperatures according to different methods has on
 297 mass balance modelling was assessed using EISModel (Cazorzi and Dalla Fontana, 1996), which
 298 was already applied to Careser and La Mare glaciers by Carturan et al. (2012a). EISModel employs

299 an enhanced temperature-index approach for computing melt, using the clear-sky shortwave
300 radiation calculated from the DEM as a distributed morpho-energetic index. The model, which is
301 suitable for applications on glaciers with limited data availability, doesn't require incoming
302 shortwave radiation measurements, which are less commonly available compared to air temperature
303 and precipitation. We tested the effect of including daily cloudiness in our mass balance
304 calculations, computing it from incoming shortwave radiation measured at Mar-gl 2973, as detailed
305 in Pellicciotti et al., (2005). As no significant changes were obtained in the efficiency statistics, we
306 assumed that the daily cloudiness could be omitted in mass balance calculations.

307 Three melt algorithms (multiplicative, additive, and extended) have been implemented and can be
308 used alternatively in EISModel. In the present work we use the additive melt algorithm, which
309 explicitly separates the thermal and radiative components:

$$310 \quad MLT_{X,t} = [TMF \cdot T_{X,t}] + [RMF \cdot CSR_{X,t}(1 - \alpha_{X,t})] \quad (11)$$

311 where TMF and RMF are empirical coefficients called the Temperature Melt Factor ($\text{mm h}^{-1} \text{ } ^\circ\text{C}^{-1}$)
312 and the Radiation Melt Factor ($\text{mm h}^{-1} \text{W}^{-1} \text{ m}^2$), $T_{X,t}$ ($^\circ\text{C}$) is the air temperature at pixel X in hour t ,
313 $CSR_{X,t}$ (W m^{-2}) is the clear sky shortwave radiation and $\alpha_{X,t}$ is the surface albedo (spatially variable
314 for ice and spatially and temporally variable for snow). For a detailed description of the model we
315 refer the reader to the work of Carturan et al. (2012a).

316 The cumulated mass balance measured at ablation stakes drilled in close proximity to the glacial
317 weather stations (AWS and VPP) served for model calibration and validation. We used alternatively
318 each of the two summer seasons of 2010 and 2011 as an independent dataset for
319 calibration/validation. Point-based EISModel calculations at the weather stations were run, using
320 four temperature series: i) measured data, ii) calculated temperature from Careser diga via the
321 standard ambient lapse rate ($-6.5^\circ\text{C km}^{-1}$), iii) calculated temperature according to the S&M
322 method, and iv) calculated temperature according to the G&B method. Option ii) is commonly used
323 in the absence of temperature data from glaciers (e.g. Gardner and Sharp, 2009; Michlmayr et al.,
324 2008; Nolin et al., 2010).

325

326 **4 Results**

327 **4.1 Seasonal characteristics of temperature data**

328 A close dependency on altitude has been detected for mean summer air temperature, both outside
329 the glaciers and, remarkably, over them (Table 2, Fig. 3). Because of thermal inversions occurring
330 at the lowermost weather station (Cog_1202) during the night and early morning, the vertical lapse
331 rate was much steeper above Car_2607 ($-8.0^\circ\text{C km}^{-1}$ in 2010 and $-8.3^\circ\text{C km}^{-1}$ in 2011) than below ($-$
332 $5.3^\circ\text{C km}^{-1}$ in 2010 and $-5.2^\circ\text{C km}^{-1}$ in 2011). At a given altitude, the on-glacier air temperature was
333 systematically lower than ambient temperature, the difference decreasing with altitude. Lapse rates
334 were also lower on the glaciers ($-7.2^\circ\text{C km}^{-1}$ in 2010 and $-6.7^\circ\text{C km}^{-1}$ in 2011), compared to high-
335 altitude off-glacier weather stations, and close to the standard ambient lapse rate ($-6.5^\circ\text{C km}^{-1}$).
336 Much shallower on-glacier lapse rates and fewer dependency of air temperature on elevation were
337 found by earlier works (e.g. Greuell and Böhm, 1998; Strasser et al., 2004; Petersen et al. 2013). As
338 reported in Table 2, the average daily temperature range and the average standard deviation are
339 largest at the valley floor and both decrease with altitude, reaching their minima over the glaciers as
340 previously reported, for example, by Oerlemans (2001). Hourly temperatures among different
341 weather stations in Val de La Mare were highly correlated ($r > 0.9$, significant at the 0.001 level),
342 with the remarkable exception of Cog_1202, at the valley floor, whose correlation with the other
343 weather stations ranged from 0.65 to 0.75, peaking at 0.84 with Car_2607.

344 4.2 Ambient temperature calculation

345 For the calculation of ambient temperature at the altitude of glaciers, which is crucial for the
346 quantification of the glacier cooling effect, we tested the following methods: i) use of a fixed
347 standard ambient lapse rate ($-6.5^{\circ}\text{C km}^{-1}$), ii) use of a fixed calibrated lapse rate (seasonal mean
348 value), and iii) use of an hourly-variable lapse rate. Methods ii) and iii) were implemented using
349 different combinations of off-glacier weather stations, calculating linear regressions of hourly
350 temperature vs. altitude. The methods were tested removing alternatively Car_3051 or Bel_3328
351 from linear regressions and using them for validation. The results, displayed in Table 3, show that
352 regardless of the method used, the inclusion of the lowermost weather station gives poorer results.
353 At Car_3051, the method iii) applied to Car_2607 and Bel_3328 works best, indicating that in our
354 case hourly variable lapse rates are the most appropriate solution while interpolating temperatures
355 between two weather stations. Conversely, method ii) applied to Car_2607 and Car_3051 provides
356 the best results at Bel_3328, which suggests that a fixed calibrated lapse rate should be used while
357 extrapolating above the uppermost station, even if uncertainty persists in these cases.

358 4.3 The glacier cooling effect

359 The cooling effect at each on-glacier weather station was calculated as the difference between the
360 measured temperature and the ambient temperature at the same elevation, computed on the basis of
361 the results described in Sect. 4.2 (i.e. hourly-variable lapse rate below Bel_3328 and fixed
362 calibrated lapse rate above it). The average seasonal cooling effect (Table 4) was maximal at Car-
363 gl_3082 (-1.01°C in 2011) and at Mar-gl_2973 (-0.74°C in 2010 and -0.90°C in 2011). Null or
364 negligible cooling was detected at Mar-gl_3438, close to the top of La Mare Glacier, and at Car-
365 gl_3144 on the small Careser Occidentale Glacier. Minor cooling occurred at Mar-gl_3215 ($-$
366 0.27°C in 2010), which was close to the balanced-budget ELA of the glacier, and at Mar-gl_3140 ($-$
367 0.47°C in 2011), in the upper ablation area. Notably, the narrow and steep terminus of La Mare
368 Glacier experienced a significant cooling effect in 2010 (-0.65°C).

369 Fig. 4 reports the mean daily cycles of the cooling effect and wind regime. A common pattern
370 emerges, with minimum cooling at night and maximum cooling around noon or in the afternoon,
371 coherent with the diurnal cycle of ambient air temperature and deriving temperature differences
372 from the glacier surface. For five out of the seven monitored sites, the cooling occurred almost
373 exclusively during daytime. Nighttime cooling took place only at Mar-gl_2973 and Car-gl_3082,
374 which are the two sites with higher mean cooling. Down-glacier winds dominated on La Mare
375 Glacier, with higher speeds compared to Careser Occidentale and Orientale glaciers, where up-
376 glacier winds prevailed. The wind speed was at its maximum at night on La Mare, especially in
377 2010, while it was at its maximum in the afternoon on the two Careser glaciers. A peculiar behavior
378 was found at the terminus of La Mare Glacier (Mar-gl_2709), where down-glacier winds dominated
379 at night, without a cooling effect, and were replaced by up-glacier winds from mid-morning to late
380 afternoon, when the cooling effect increased sharply. Wind data were not available at Mar-gl_3438,
381 due to instrumentation failure, but we can argue that katabatic winds were not prevalent at this site,
382 which is close to the crest, based on results published for similar locations in previous works (e.g.
383 Greuell et al., 1997; Strasser et al., 2004).

384 Different weather conditions led to a considerable temporal variability of the glacier cooling effect
385 during the two summer seasons of 2010 and 2011 (Fig. 5). Cooling was maximal during warm
386 anticyclonic periods and nearly absent during cold unsettled weather. Differences among sites
387 increased with warmer temperatures, whereas they nearly disappeared during cold and unstable
388 periods. The highest variations occurred at Mar-gl_2973, Mar-gl_3215, Mar-gl_3140, and Car-
389 gl_3082 while at Mar-gl_3438 and Car-gl_3144 there was a smaller temporal variability. A
390 warming, rather than cooling, effect was observed on some days, mainly at the upper weather
391 stations of La Mare Glacier. A close check on the wind and temperature data revealed that this was

392 ascribable to local föhn conditions, that is, forced adiabatic heating brought by strong northerly
393 winds.

394 4.4 Calculation of on-glacier temperature from off-site data

395 According to the S&M method, piecewise linear regressions of on-glacier hourly temperature
396 versus ambient temperature at the same elevation have been calculated for each glacial weather
397 station. The values of the parameters k_1 and k_2 (i.e. temperature sensitivities for ambient
398 temperatures below and above the threshold temperature T^* , respectively) were well aligned with
399 the transfer functions proposed by S&M, using the FPL as predictor (Fig. 6). On the other hand, the
400 transfer function for T^* suggested by S&M, using station elevation as a predictor, could not be used
401 in AVDM given the different geographic and climatic setting of the two study areas. We therefore
402 propose to substitute Eq. (2) with the following function:

$$403 T^* = \frac{a \cdot FPL}{b + FPL} \quad (12)$$

404 which uses the FPL (m) rather than elevation as a predictor, thus being potentially more
405 generalizable. The outlier already excluded by S&M was not included in our calculation of Eq. (12),
406 nor was Mag-gl_2709, both due to under-sampling at below-zero temperatures. Fig. 6 shows data
407 points, transfer functions, and parameters. Calculated versus measured temperature is shown in Fig.
408 7 along with related statistics. Four out of the five sites where the method works satisfactorily (ME
409 $< 0.5^\circ\text{C}$ in absolute value and $N\&S$ index > 0.87) have prevailing katabatic winds. On the contrary,
410 lower performance affects sites close to the glacier margin (Mar-gl_3438 and, in particular, Mar-
411 gl_2709), where katabatic winds are disrupted by valley winds or synoptic winds, and Car-gl_3082,
412 where up-glacier winds prevail. The efficiency statistics for all sites are: $ME = -0.06^\circ\text{C}$, $RMSE =$
413 0.73°C and $N\&S = 0.692$.

414 According to the G&B method, the location x_0 where the air enters the glacier wind layer, and the
415 length scale L_R , can be calculated by an exponential function which expresses the 'climatic
416 sensitivity' in function of the distance x along the flowline:

$$417 \frac{dT(x)}{dT_{CS}} = \exp\left(-\frac{x+x_0}{L_R}\right) \quad (13)$$

418 Climatic sensitivities were calculated, comparing daily mean temperature at our on-glacier sites to
419 daily mean temperature at Car_3051, and have been added for comparison to the data displayed in
420 Figure 5 of the Greuell and Böhm (1998) paper. The results are shown in Fig. 8 and indicate a fairly
421 good alignment of our data with the other glaciers' data and with the best fit calculated by G&B for
422 the Pasterze weather stations. It therefore seemed appropriate to use the values of x_0 and L_R
423 calculated by those authors, that is, 1440 and 8340 m respectively. According to the G&B
424 procedure, the hourly temperature above the freezing level was set equal to the ambient temperature
425 (Sect. 4.2). Below the freezing level, the glacier-wind model of G&B was applied, setting i) $x_0 = 0$
426 if the freezing level was below the top of the flowline, and ii) $x_0 = 1440$ m if it was above this point,
427 in order to take into account a climate sensitivity < 1 at the top of the flowline. z_0 was set equal to
428 the freezing level in case i) and equal to the altitude of the top of the flowline in case ii). These
429 settings are the same as those used in the G&B paper. Nevertheless, no corrections were applied to
430 the computed temperatures, as was done by G&B, who applied a fixed offset of -0.74°C .

431 Fig. 9 displays the results of the G&B method. Calculated temperatures matched the measured
432 temperatures fairly well and the efficiency statistics for all sites were better than for the S&M
433 method: $ME = -0.27^\circ\text{C}$, $RMSE = 0.40^\circ\text{C}$, $N\&S = 0.908$. Improvements were observed, in particular,
434 at Mar-gl_2709, Car-gl_3082, and Mar-gl_3438, even if these sites lack predominant katabatic
435 winds. A clear step is observable at Mar-gl_2709 and, slightly less obvious, at Mar-gl_2973 in both

436 summer 2010 and 2011, attributable to the jump of x_0 from 0 to 1440 m when the freezing level
437 exceeds the top of the flowline.

438

439 **4.5 Mass balance modeling**

440 EISModel applications using measured temperature datasets resulted in RMSE values well below
441 the mass balance measurement error from ablation stakes readings (~200 mm w.e., Thibert et al.,
442 2008; Huss et al., 2009), thus confirming the good skill of the modeling tool. On the other hand, the
443 RMSE was nearly double when calculated temperature datasets were used as input, and
444 considerable differences also exist in the calibration parameters (Table 5).

445 The spatial distribution of modeling errors using temperature extrapolations from Car_2607 via the
446 standard lapse rate (Fig. 10, scatterplots b1 to b4) replicated the findings of Carturan et al. (2012a)
447 for the six previous years (2004 to 2009). In particular, the modeled vertical gradient of mass
448 balance on La Mare Glacier in summer 2010 was lower than the observed one, in both calibration
449 and validation runs, due to uneven errors in estimating air temperature (+0.77, +1.17, and +1.14°C
450 at Mar-gl_2709, Mar-gl_2973, and Mar-gl_3215 respectively). This dataset of overestimated
451 temperatures led to significantly lower calibration parameters compared to the measured
452 temperature dataset. Moreover, including critical points close to the lower margin of the glacier
453 (Mar-gl_2709 in summer 2010) led to wrong calibration at the other two points, which are likely to
454 have a higher spatial representativeness given the larger distance from the glacier margin.

455 The calibration parameters obtained with the G&B temperature dataset were closer to those
456 obtained with the measured temperature dataset, as could be expected given the smaller errors in
457 temperature estimations (Fig. 9). In summer 2010, modeling results with the G&B temperature
458 dataset were also the best among the three tested methods for air temperature calculation, in both
459 calibration and validation runs. The same cannot be stated for summer 2011, due to the larger
460 temperature underestimation at Mar-gl_3140 and Car-gl_3144. Similar errors occurring at Mar-
461 gl_3438 did not impact mass balance estimations because they mainly happened at below-zero
462 temperatures (Fig. 9).

463 The S&M temperature dataset led to the worst results in summer 2010 due to the strong
464 underestimation of air temperature at Mar-gl_2709 (-1.6°C). Calibrated parameters in 2010 were
465 thus overestimated and led to mass balances that were too negative, on average, in 2011. On the
466 contrary, when used for calibration, the data of 2011 led to parameters much closer to the measured
467 temperature dataset, leading to correct mass balance estimations in summer 2010 with the exception
468 of the already mentioned Mar-gl_2709.

469

470 **5 Discussion**

471 The temperature distribution and wind regime were found to be remarkably different for the three
472 investigated glaciers (Tables 2 and 4, Fig. 4). The most significant differences were detected
473 between La Mare Glacier, where the KBL and the cooling effect were clearly recognizable, and the
474 Careser Occidentale Glacier, where the air temperature was not significantly different from the
475 ambient temperature and where prevailing up-glacier winds (i.e. valley winds) dominated.
476 Differences were even more prominent during warm and stable weather (Fig. 5), brought by
477 persistent anticyclonic systems (as detected by inspection of reanalysis weather charts from
478 www.wetterzentrale.de, last access: 31 October 2014).

479

480 The Car-gl_3082 site, on Careser Orientale Glacier, also displayed peculiar conditions compared to
481 most weather stations operated on La Mare Glacier. On the one hand a prevailing up-glacier wind
482 was recognized, but it cannot be attributed unequivocally to valley winds because the direction
483 roughly corresponds to prevailing synoptic winds in the Ortles-Cevedale area (Gabrieli et al., 2011).
484 The occurrence of weaker local winds and more relevant entrainment of synoptic winds have been
485 hypothesized, for example, by Ayala et al., (2015), for glaciers without a well-defined tongue. On
486 the other hand, although katabatic flows were generally absent, this site was the coldest in summer
487 2011, exhibiting a mean depression of 1°C compared to the ambient temperature (Table 4). In
488 addition, during warm anticyclonic periods it displayed a cooling effect similar to Mar-gl_2973 and
489 Mar-gl_3140, located in the middle part of La Mare Glacier. This is unusual for locations close to
490 the top of glacier flowlines, which normally display a low cooling effect and high temperature
491 sensitivity (e.g. Greuell and Böhm, 1998; Shea and Moore, 2010; Petersen et al., 2013). The
492 efficient cooling at Car-gl_3082 could have been caused by the combination of adiabatic cooling of
493 ascending air and cooling by loss of sensible heat due to the rather long fetch (780 m from the lower
494 edge of the glacier), whereas in katabatic flows the loss of sensible heat is to some extent
495 compensated by the adiabatic heating of descending air (Greuell and Böhm, 1998).

496 The behavior of the two weather stations on Careser Occidentale and Orientale glaciers provides
497 evidence of the reduced effectiveness of small glaciers (deriving from the fragmentation of larger
498 glaciers) in cooling the air above, compared to wider glaciers or wider portions of the same parent
499 glacier. This is suggested by the fact that these two weather stations (Car-gl_3082 and Car-gl_3144),
500 despite being at almost the same flow path distance from the upper glacier margin (Table 1, Fig. 2),
501 have very different cooling effects (Table 4, Fig. 4), which largely explain errors in modeled
502 ablation rates (Fig. 10; Figure 8 from Carturan et al., 2012).

503 In consideration of the high number and contribution to the world's total ice volume of smaller
504 glaciers (Haeberli et al., 1989; Paul et al., 2004; Zemp et al., 2008; Bahr and Radić, 2012), and
505 given the absence of previous experimental data from such small ice bodies, these results provide a
506 first quantification for an important reinforcing mechanism during glacier decay, that is, the
507 disintegration of parent glaciers into smaller units, which have reduced effectiveness in cooling the
508 air above and in triggering katabatic flows. Clearly, these results are not conclusive and require
509 further experimental data to assess their generalizability, and to develop generalized strategies for
510 calculating air temperature over glaciers with similar characteristics, to be implemented in
511 distributed mass balance models.

512 A clear dependency of air temperature on elevation was found on La Mare Glacier, where the
513 weather stations were placed along a longitudinal profile, exploring a large range of elevations (Fig.
514 3). The on-glacier lapse rate was steeper than the standard ambient lapse rate, unlike in previous
515 works which mostly report lower-shallower values, ranging from -2.8 to -8.1°C km⁻¹ and averaging
516 -4.9°C km⁻¹ (Petersen and Pellicciotti, 2011, and references cited therein; Petersen et al., 2013). The
517 high-steep lapse rate measured on La Mare Glacier is likely due to its physical characteristics and to
518 the specific location of weather stations. For example, Mar-gl_2973, which is located 2.13 km
519 downslope from the upper margin of the glacier, displayed only a moderate cooling effect (-0.74°C
520 in 2010 and -0.90°C in 2011), due to the presence of a steep slope causing adiabatic heating right
521 above the weather station. An even more unusual behavior was measured at Mar-gl_2709, close to
522 the terminus of the glacier. Here the cooling effect was detected only during daytime, with valley
523 winds prevailing over katabatic winds, while at night the adiabatic heating of the air descending the
524 steep tongue prevailed over the cooling due to turbulent exchanges. Besides the physical
525 characteristics of the glacier, however, the steep lapse rates might also have been influenced by the
526 high-steep lapse rate measured outside the thermal influence of glaciers.

527 The specific reasons for the steepness of the high-altitude ambient lapse rates are not easy to
528 identify. According to Marshall et al. (2007) and Minder et al. (2010), for example, they could have
529 been caused by the prevailing synoptic circulation, local energy balance regime, persistence of
530 snow cover, geographic position (windward or leeward with respect to the prevailing synoptic
531 wind). Apart from these considerations, it has to be noted that the interpolation and extrapolation of
532 ambient temperature at high altitudes, as a starting point for the computation of the on-glacier
533 temperature fields, are strongly dependent on the availability and/or selection of suitable weather
534 stations. As already suggested e.g. by Oerlemans, (2001), measurements from high-altitude weather
535 stations are preferable to measurements from valley-floor sites, which are prone to thermal
536 inversions and subject to high temperature oscillations during the day.

537 The good alignment of our data points with the transfer functions of Shea and Moore (2010), which
538 can be seen in Fig. 6, is remarkable given the different characteristics of glaciers and geographic
539 setting of the two study areas. This result points to a good generalizability of the S&M method,
540 which we have tried to improve by implementing a transfer function for T^* based on the *FPL* rather
541 than on elevation. The S&M method was fairly successful at sites where the KBL was detected
542 (Mar-gl_3140, Mar-gl_3215), that is, for the conditions under which the method has been
543 implemented. Nevertheless, at Mar-gl_2973 it significantly underestimated the temperature,
544 probably because it does not account for gradients upslope of the weather station, which causes a
545 local prevalence of adiabatic heating. A larger error occurred at Mar-gl_2709, which is however
546 influenced by valley winds and thermal emission from the surrounding bare rocks, determining high
547 temperature sensitivity and unusual T^* at such a long *FPL* (2896 m, Fig. 6). With this method it was
548 not possible to reproduce the temperature differences between Car-gl_3082 and Car-gl_3144, as
549 expected, because they have similar values of down-glacier *FPL* (313 and 354 m, respectively).

550 The G&B method provided the best overall results. Among sites with prevailing katabatic winds,
551 the improvement was clearest at Mar-gl_2973, where the method was able to account for the
552 combined effect of adiabatic heating and turbulent exchanges, which were regulated by the slope
553 variations along the upstream flowline. On the other hand, it was worse than the S&M method at
554 distinguishing between the two Careser glaciers, and the better results in terms of lower mean errors
555 at Mar-gl_2709, Mar-gl_3438 and Car-gl_3082, compared to the S&M method, are coincidental
556 because at these sites the KBL was almost absent or not prevailing.

557 Other combinations of parameters x_0 and L_R have been tested to evaluate whether they are valid
558 alternatives, for example for eliminating the artificial step in calculated versus observed temperature
559 at Mar-gl_2973 and Mar-gl_2709 (Fig. 9), caused by the jump of x_0 from 0 to 1440 m when the
560 freezing level exceeds the top of the flowline. The tested combinations were: i) $x_0 = 0$ m (constant)
561 and $L_R = 8340$ m, ii) $x_0 = 1440$ m (constant) and $L_R = 8340$ m, and iii) $x_0 = 1835$ m (constant) and L_R
562 = 12682 m. The last combination results from the best fit to AVDM data in Fig. 8, excluding the
563 outlier Mar-gl_2709. We also tested the calculation using the unmodified ambient temperature.
564 Tests indicate that at sites with almost no cooling effect (Mar-gl_3438 and Car-gl_3144) the
565 unmodified ambient temperature or the combination i) ($x_0 = 0$) provide the best results (mean errors
566 $< 0.2^\circ\text{C}$ in absolute value). At the four sites with prevailing KBL the best overall solution was iii),
567 but this combination is specific for the AVDM and not generalizable, due to the rather small size of
568 our glaciers. At Mar-gl_2973, options ii) and iii) completely removed the step and provided the best
569 statistics. At Mar-gl_3215, option iii) provided almost identical results to a variable x_0 , while
570 options i) and ii) led to excessive overestimations and underestimations, respectively. At Mar-
571 gl_3140, the best option was iii).

572 These findings highlight site-specific and glacier-specific conditions which still need investigation
573 in order to generalize the G&B procedure, possibly by including smaller or disintegrating glaciers
574 in the datasets used for the generalization. Sites where the KBL no longer exists and is replaced by

575 prevailing valley winds and/or synoptic winds also need to be included as they reveal important
576 controlling mechanisms during glacier shrinking, which require modifications to the main G&B
577 algorithms in order to be taken into account.

578 The results of EISModel applications underline the importance of correct on-glacier air temperature
579 estimation for reliable mass balance calculations (Table 5, Fig. 10). Even small estimation errors
580 induce significant distortions in calibration parameters and compromise model generalizability. The
581 2010 dataset on La Mare Glacier clearly demonstrates how single points, especially if they are
582 displaced along altitudinal profiles, can affect the calibration of the model and its capability to
583 account for the vertical gradients of the mass balance. This problem is clearly emphasized in our
584 case study, with only three weather stations along the flowline of La Mare Glacier in 2010. The
585 spatial representativeness of Mar-gl_2973 and Mar-gl_3215 is likely much higher than that of Mar-
586 gl_2709, at the glacier terminus, which reflects the conditions close to the lower edge of glaciers.
587 However, mass balance models should be improved in order to account for the decreased thermal
588 offset in these areas and in smaller glacier units resulting from the fragmentation of larger glaciers,
589 because they represent important processes involved in the response of glaciers to climatic changes.

590

591 **6 Concluding remarks**

592 The results of this work have interesting implications for the knowledge of glacier's reactions to
593 climatic changes, and for their modeling. The main conclusions from this study are the following:

- 594 1) our findings provide a first experimental evidence for the reduced effectiveness of small
595 glaciers ($< 0.5 \text{ km}^2$) in cooling the air above and in triggering katabatic flows. This
596 represents an important reinforcing mechanism during glacier decay and fragmentation.
- 597 2) a good match between our temperature measurements and the parameterizations proposed
598 by Shea and Moore (2010) and, best of all, Greuell and Böhm (1998) was found, at least for
599 the on-glacier weather stations where katabatic flows prevail. This represents a step forward
600 for the generalization of these methods, which on the other hand still need refinements, in
601 particular for areas close to the margins (e.g. the front) and for the smaller units resulting
602 from glacier fragmentation
- 603 3) even small deviations of calculated on-glacier temperature from observations significantly
604 impacted the calibration of EISModel and its efficiency, thus confirming that accurate
605 temperature estimations are an essential prerequisite for model development, calibration and
606 generalizability.

607

608 **Author contribution**

609 L. Carturan, F. Cazorzi and G. Dalla Fontana designed the glacio-meteorological experiment and
610 carried it out. L. Carturan and F. De Blasi processed and analyzed the experimental data. F. Cazorzi
611 and L. Carturan developed the EISModel and performed the glacier mass balance simulations. L.
612 Carturan prepared the manuscript with contributions from all co-authors.

613 **Acknowledgments**

614 The data and the mass balance model used in this study can be made available upon request to the
615 authors. This study was funded by the Italian MIUR Project (PRIN 2010-11): "Response of
616 morphoclimatic system dynamics to global changes and related geomorphological hazards" (local

617 and national coordinators G. Dalla Fontana and C. Baroni). The authors acknowledge the
618 Autonomous Province of Trento and Enel SpA for providing the meteorological and topographic
619 data. Special thanks to Vinicio Carraro for the help in the setup of automatic weather stations, and
620 to the students, colleagues and alpine guides who have contributed to the field surveys. Finally,
621 thanks to the scientific editor V. Radić and to two anonymous reviewers, whose comments were
622 helpful for finalizing the paper.

623

624 **References**

625 Abbate, S., Avvenuti, M., Carturan, L., and Cesarini, D.: Deploying a communicating automatic
626 weather station on an Alpine Glacier, *Procedia Comput. Sci.*, 19, 1190–1195, 2013.

627 [Ayala, A., Pellicciotti, F., and Shea, J. M.: Modeling 2 m air temperatures over mountain glaciers:
628 Exploring the influence of katabatic cooling and external warming. *J. Geophys. Res. Atmos.*, 120,
629 doi:10.1002/2015JD023137, 2015.](#)

630 Bahr, D. B., and Radić, V.: Significant contribution to total mass from very small glaciers. *The*
631 *Cryosphere*, 6, 763–770, 2012.

632 Barry, R. G.: The status of research on glaciers and global glacier recession: a review, *Prog. Phys.*
633 *Geog.*, 30(3), 285-306, 2006.

634 Braithwaite, R. J.: Regional modelling of ablation in West Greenland, *Grøn. Geol. Unders. Rapp.*
635 98, 20 pp., 1980.

636 Braithwaite, R. J., Zhang, Y., and Raper, S. C. B.: Temperature sensitivity of the mass balance of
637 mountain glaciers and icecaps as a climatological characteristic, *Z. Gletscherkunde Glazialgeol.*, 38,
638 35–61, 2002.

639 Carturan, L.: Climate change effects on the cryosphere and hydrology of a high-altitude watershed.
640 PhD diss., TeSAF - University of Padova, Italy, 2010.

641 Carturan, L., Dalla Fontana, G., and Cazorzi, F.: The mass balance of La Mare Glacier (Ortles-
642 Cevedale, Italian Alps) from 2003 to 2008, in: *Epitome - Geoitalia 2009*, Settimo Forum Italiano di
643 Scienze della Terra, Rimini, Italy, 9–11 September 2009, Vol. 3, p. 298, 2009.

644 Carturan, L., Cazorzi, F., and Dalla Fontana, G.: Distributed mass-balance modeling on two
645 neighboring glaciers in Ortles-Cevedale, Italy, from 2004 to 2009, *J. Glaciol.*, 58(209), 467-486,
646 2012a.

647 Carturan L., Dalla Fontana, G., and Borga, M.: Estimation of winter precipitation in a high-altitude
648 catchment of the Eastern Italian Alps: validation by means of glacier mass balance observations,
649 *Geogr. Fis. Din. Quat.*, 35, 37-48, 2012b.

650 Carturan, L., Baroni, C., Becker, M., Bellin, A., Cainelli, O., Carton, A., Casarotto, C., Dalla
651 Fontana, G., Godio, A., Martinelli, T., Salvatore, M. C., and Seppi R.: Decay of a long-term
652 monitored glacier: Careser Glacier (Ortles-Cevedale, European Alps), *The Cryosphere*, 7, 1819-
653 1838, 2013.

654 Carturan L., Baroni, C., Carton, A., Cazorzi, F., Dalla Fontana, G., Delpero, C., Salvatore, M. C.,
655 Seppi, R., and Zanoner, T.: Reconstructing fluctuations of La Mare Glacier (Eastern Italian Alps) in
656 the Late Holocene: new evidences for a Little Ice Age maximum around 1600 AD, *Geografiska*
657 *Annaler: Series A, Physical Geography*, 96, 287-306, 2014.

- 658 Cazorzi, F. and Dalla Fontana, G.: Snowmelt modeling by combining air temperature and a
659 distributed radiation index, *J. Hydrol.*, 181(1–4), 169–187, 1996.
- 660 Charbonneau, R., Lardeau, J. P., and Obled, C.: Problems of modelling a high mountainous
661 drainage basin with predominant snow yields, *Hydrol. Sci. Bull.*, 26(4), 345–361, 1981.
- 662 Davidovich, N. V. and Ananicheva, M. D.: Prediction of possible changes in glacio-hydrological
663 characteristics under global warming: Southeastern Alaska, USA, *J. Glaciol.*, 42(142), 407–412,
664 1996.
- 665 Eriksson, B. E.: Glaciological investigations in Jotunheimen and Sarek in the years 1955 to 1957.
666 *Geographica*, 34, 208 pp., 1958.
- 667 Fischer, A.: Glaciers and climate change: Interpretation of 50 years of direct mass balance of
668 Hintereisferner, *Global Planet. Change*, 71 (1-2), 13–26, 2010.
- 669 Gabrieli J., Carturan, L., Gabrielli, P., Turetta, C., Cozzi, G., Staffler, H., Dinale, R., Dalla Fontana,
670 G., Thompson, L., and Barbante, C.: Impact of Po Valley emissions on the highest glacier of the
671 Eastern European Alps, *Atmos. Chem. Phys.*, 11, 8087–8102, 2011.
- 672 Gardner, A. S. and Sharp, M. J.: Sensitivity of net mass-balance estimates to near-surface
673 temperature lapse rates when employing the degree-day method to estimate glacier melt, *Ann.*
674 *Glaciol.*, 50, 80–86, 2009.
- 675 Gardner, A. S., Sharp, M. J., Koerner, R. M., Labine, C., Boon, S., Marshall, S. J., Burgess, D. O.,
676 and Lewis, D.: Near-surface temperature lapse rates over arctic glaciers and their implications for
677 temperature downscaling, *J. Clim.*, 22, 4281–4298, 2009.
- 678 Georges, C. and Kaser, G.: Ventilated and unventilated air temperature measurements for glacier-
679 climate studies on a tropical high mountain site, *J. Geophys. Res.*, 107(D24), 4775,
680 doi:10.1029/2002JD002503, 2002.
- 681 Greuell, W. and Böhm, R.: 2m temperatures along melting midlatitude glaciers, and implications
682 for the sensitivity of the mass balance to variations in temperature, *J. Glaciol.*, 44(146), 9–20, 1998.
- 683 Greuell, W., Knap, W. H., and Smeets, P. C.: Elevational changes in meteorological variables along
684 a mid-latitude glacier during summer, *J. Geophys. Res.*, 102(D22), 25941–25954, doi:
685 10.1029/97JD02083, 1997.
- 686 Haeberli, W., Bosch, H., Scherler, K., Østrem, G. and Wallén, C. (eds): World Glacier Inventory:
687 Status 1988. IAHS(ICSJ)/UNEP/UNESCO/World Glacier Monitoring Service, Nairobi, 1989.
- 688 Haeberli, W., Hoelzle, M., Paul, F., and Zemp, M.: Integrated monitoring of mountain glaciers as
689 key indicators of global climate change: the European Alps, *Ann. Glaciol.*, 46(1), 150–160, 2007.
- 690 Havens, J. M.: Climatological Notes from Axel Heiberg Island, NWT, Canada, *Arctic*, 17(4), 261-
691 263, 1964.
- 692 Hock, R.: Glacier melt: a review of processes and their modelling, *Prog. Phys. Geog.*, 29(3), 362-
693 391, 2005.
- 694 Huss, M., Bauder, A., and Funk, M.: Homogenization of longterm mass-balance time series, *Ann.*
695 *Glaciol.*, 50(50), 198–206, 2009.
- 696 Khodakov, V. G.: Glaciers as water resource indicators of the glacial areas of the USSR.
697 International Association of Hydrological Sciences Publication, 104, 22–29, 1975.

- 698 Klok, E. J. and Oerlemans, J.: Modelled climate sensitivity of the mass balance of
699 Morteratschgletscher and its dependence on albedo parameterization, *Int. J. Climatol.*, 24, 231–245,
700 2004.
- 701 Machguth, H., Purves, R. S., Oerlemans, J., Hoelzle, M., and Paul, F.: Exploring uncertainty in
702 glacier mass balance modelling with Monte Carlo simulation, *The Cryosphere*, 2, 191–204, 2008.
- 703 Marshall, S. J., Sharp, M. J., Burgess, D. O., and Anslow, F. S.: Near surface-temperature lapse
704 rates on the Prince of Wales Icefield, Ellesmere Island, Canada: implications for regional
705 downscaling of temperature, *Int. J. Climatol.*, 27(3), 385–398, 2007.
- 706 Michlmayr, G., Lehning, M., Koboltschnig, G., Holzmann, H., Zappa, M., Mott, R., and Schonert,
707 W.: Application of the alpine 3D model for glacier mass balance and glacier runoff studies at
708 Goldbergkees, Austria, *Hydrol. Process.*, 22, 3941–3949, 2008.
- 709 Minder, J. R., Mote, P. W., and Lundquist, J. D.: Surface temperature lapse rates over complex
710 terrain: Lessons from the Cascade Mountains, *J. Geophys. Res.*, 115, D14122, doi:
711 10.1029/2009JD013493, 2010.
- 712 Nash, J. E. and Sutcliffe, J. V.: River flow forecasting through conceptual models. Part 1. A
713 discussion of principles, *J. Hydrol.*, 10(3), 282–290, 1970.
- 714 Nolin, A., Philippe, J., Jefferson, A., and Lewis, S. L.: Present-day and future contributions of
715 glacier runoff to summertime flows in a Pacific Northwest watershed: Implications for water
716 resources, *Water Resour. Res.*, 46, W12509, doi: 10.1029/2009WR008968, 2010.
- 717 Oerlemans, J.: *Glaciers and climate change*, AA Balkema, Lisse, 2001.
- 718 Paul, F.: The influence of changes in glacier extent and surface elevation on modeled mass balance,
719 *The Cryosphere*, 4, 569–581, 2010.
- 720 Paul, F., Kääb, A., Maisch, M., Kellenberger, T. and Haeberli, W.: Rapid disintegration of Alpine
721 glaciers observed with satellite data. *Geophys. Res. Lett.*, 31, L21402, 2004.
- 722 Paul, F., Machguth, H., and Kääb, A.: On the impact of glacier albedo under conditions of extreme
723 glacier melt: the summer of 2003 in the Alps, *EARSeL eProc.*, 4(2), 139–149, 2005.
- 724 Petersen, L. and Pellicciotti, F.: Spatial and temporal variability of air temperature on a melting
725 glacier: atmospheric controls, extrapolation methods and their effect on melt modeling, *Juncal
726 Norte Glacier, Chile*, *J. Geophys. Res.*, 116(D23), D23109, doi: 10.1029/2011JD015842, 2011.
- 727 Petersen, L., Pellicciotti, F., Juszak, I., Carenzo, M., and Brock, B.: Suitability of a constant air
728 temperature lapse rate over an Alpine glacier: testing the Greuell and Böhm model as an alternative,
729 *Ann. Glaciol.*, 54(63), 120–130, 2013.
- 730 Raymond, C. F. and Neumann, T. A.: Retreat of Glaciar Tyndall, Patagonia, over the last half-
731 century, *J. Glaciol.*, 51(173), 239–247, 2005.
- 732 Savenije, H. H. G.: Equifinality, a blessing in disguise? *Hydrol. Process.*, 15(14), 2835–2838, 2001.
- 733 Schytt, V.: *Glaciological investigations in the Thule camp area*, S.I.P.R.E. Report No. 28, 88 pp.,
734 1955.
- 735 Shea, J. M. and Moore, R. D.: Prediction of spatially distributed regional-scale fields of air
736 temperature and vapor pressure over mountain glaciers, *J. Geophys. Res.*, 115, D23107,
737 doi:10.1029/2010JD014351, 2010.

- 738 Sivapalan, M.: Pattern, process and function: elements of a unified theory of hydrology at the
739 catchment scale, in: Encyclopedia of hydrological sciences, Anderson, M. G. and McDonnell, J. J.
740 eds., Vol. 1. Wiley, Chichester, 193–219, 2006.
- 741 Small, E. E.: Hypsometric forcing of stagnant ice margins: Pleistocene valley glaciers, San Juan
742 Mountains, Colorado, *Geomorphology*, 14, 109–121, 1995.
- 743 Strasser, U., Corripio, J., Pellicciotti, F., Burlando, P., Brock, B., and Funk, M.: Spatial and
744 temporal variability of meteorological variables at Haut Glacier d’Arolla (Switzerland) during the
745 ablation season 2001: measurements and simulations, *J. Geophys. Res.*, 109(D3), D3103, doi:
746 10.1029/2003JD003973, 2004.
- 747 Tarboton, D. G., Bras, R. L., and Rodriguez-Iturbe, I.: On the extraction of channel networks from
748 digital elevation data. *Hydrol. Process.*, 5(1), 81-100, 1991.
- 749 Thibert, E., Blanc, R., Vincent, C., and Eckert, N.: Glaciological and volumetric mass-balance
750 measurements: error analysis over 51 years for Glacier de Sarennes, French Alps, *J. Glaciol.*,
751 54(186), 522–532, 2008.
- 752 van den Broeke, M. R.: Momentum, heat, and moisture budgets of the katabatic wind layer over a
753 midlatitude glacier in summer, *J. Appl. Meteorol.*, 36(6), 763-774, 1997.
- 754 World Meteorology Organization (WMO): Intercomparison of models for snowmelt runoff,
755 Operational Hydrology Report 23 (WMO no. 646), 1986.
- 756 Zanon, G.: Recent glaciological research in the Ortles- Cevedale region (Italian Alps), *Geogr. Fis.*
757 *Din. Quat.*, 5(1), 75–81, 1982.
- 758 Zemp, M., Paul, F., Hoelzle, M. and Haeberli, W.: Glacier fluctuations in the European Alps 1850–
759 2000: an overview and spatio-temporal analysis of available data. In: Orlove, B., Wiegandt, E. and
760 Luckman B., (eds), *The Darkening Peaks: Glacial Retreat in Scientific and Social Context*.
761 University of California Press, Berkeley, 152–167, 2008.

762

Tables

764 **Table 1.** Location, flow path length (*FPL*), period of observation and used variables for glacier and
 765 ambient weather stations^a. The periods with common records are 3 July to 23 September 2010 and 7
 766 July to 12 September 2011.

Weather station	Easting (m)	Northing (m)	Elevation (m a.s.l.)	<i>FPL</i> (m)	Period of observation		Used variables
					Summer 2010	Summer 2011	
La Mare Glacier							
Mar-gl_2709	626692	5143668	2709	2896	x		T, W
Mar-gl_2973	625960	5143483	2973	2132	x	x	T, W
Mar-gl_3215	625205	5143101	3215	1278	x		T, W
Mar-gl_3140	625290	5143523	3140	805		x	T, W
Mar-gl_3438	624199	5142924	3438	40	damaged	x	T, W
Careser Glacier							
Car-gl_3082	632283	5145512	3082	313		x	T, W
Car-gl_3144	629690	5145375	3144	354		x	T, W
Ambient weather stations							
Cog_1202	629915	5135988	1202	\	x	x	T
Car_2607	630570	5142410	2607	\	x	x	T, P
Car_3051	630799	5145553	3051	\	x	x	T
Bel_3328	624957	5151212	3328	\	x	x	T

767 ^aT = air temperature, W = wind speed and direction, P = precipitation. On-glacier sites are in bold
 768 type.

769

770

771

772

773

774

775

776

777

778

779

780

781

782

783

784 **Table 2.** Descriptive statistics for air temperature data recorded by the weather stations. On-glacier
 785 sites are in bold type.

Weather station	Minimum	Maximum	Mean	Standard deviation	Mean daily range
Summer 2010					
Mar-gl_2709	-1.9	14.2	5.9	3.3	2.2
Mar-gl_2973	-4.4	11.6	3.8	3.1	2.5
Mar-gl_3215	-6.6	10.6	2.2	3.4	2.9
Cog_1202	2.3	29.8	14.8	5.5	10.2
Car_2607	-2.4	18.4	7.3	4.1	4.6
Car_3051	-5.6	14.1	3.9	4.0	2.8
Bel_3328	-10.5	13.9	1.5	4.5	3.6
Summer 2011					
Mar-gl_2973	-4.8	12.0	4.3	2.7	2.6
Mar-gl_3140	-6.2	9.7	3.3	2.8	2.1
Mar-gl_3438	-7.9	9.5	1.1	3.1	3.2
Car-gl_3082	-6.0	10.8	3.3	2.9	2.6
Car-gl_3144	-6.1	10.9	3.5	3.1	2.3
Cog_1202	4.0	29.8	15.4	4.9	10.5
Car_2607	-0.9	19.5	8.1	3.6	4.9
Car_3051	-5.3	13.7	4.6	3.5	2.8
Bel_3328	-8.2	13.5	2.1	3.8	3.5

786

787

788

789

790

791

792

793

794

795

796

797

798

799

800

801

802

803 **Table 3.** Validation statistics for ambient temperature calculations (global dataset including summer
 804 2010 and 2011)^a

Lapse rate (°C m ⁻¹)	Used weather stations	Calculation of air temperature at Car_3051			Calculation of air temperature at Bel_3328		
		Mean Error (°C)	RMSE (°C)	N&S index	Mean Error (°C)	RMSE (°C)	N&S index
Moist adiabatic lapse rate							
-0.0065	1	-1.14	3.81	-0.019	-0.51	3.59	0.276
-0.0065	2	0.59	1.32	0.878	1.22	2.02	0.771
-0.0065	3	\	\	\	0.63	1.46	0.880
-0.0065	4	-0.63	1.46	0.851	\	\	\
Fixed calibrated lapse rate							
-0.0053	1, 2	1.13	1.64	0.812	2.11	2.65	0.605
-0.0059	1, 3	\	\	\	0.81	1.54	0.866
-0.0063	1, 4	-0.70	1.49	0.845	\	\	\
-0.0078	2, 3	\	\	\	0.27	1.34	0.899
-0.0082	2, 4	-0.17	1.32	0.877	\	\	\
-0.0057	1, 2, 3	\	\	\	0.85	1.56	0.863
-0.0061	1, 2, 4	-0.74	1.51	0.841	\	\	\
Hourly variable lapse rate							
Hourly variable	1, 2	1.13	1.55	0.831	2.11	2.89	0.529
Hourly variable	1, 3	\	\	\	0.81	1.74	0.830
Hourly variable	1, 4	-0.70	1.51	0.840	\	\	\
Hourly variable	2, 3	\	\	\	0.27	1.64	0.849
Hourly variable	2, 4	-0.17	1.01	0.929	\	\	\
Hourly variable	1, 2, 3	\	\	\	0.85	1.76	0.826
Hourly variable	1, 2, 4	-0.74	1.55	0.831	\	\	\

805 ^aWeather stations: 1 = Cog_1202, 2 = Car_2607, 3 = Car_3051, 4 = Bel_3328. N&S index is the
 806 efficiency criterion according to Nash and Sutcliffe (1970). Bold type indicates the best results for
 807 each tested method.

808
 809
 810
 811
 812
 813
 814
 815
 816
 817
 818
 819

820 **Table 4.** Mean values of cooling effect, wind speed and wind direction recorded at the on-glacier
 821 weather stations.

Weather station	Mean cooling effect (°C)	Mean wind speed (m/s)	Mean wind direction (°)
Summer 2010			
Mar-gl_2709	-0.65	2.00	247
Mar-gl_2973	-0.74	3.13	230
Mar-gl_3215	-0.27	3.47	258
Summer 2011			
Mar-gl_2973	-0.90	2.82	224
Mar-gl_3140	-0.47	3.00	239
Mar-gl_3438	0.06	\	\
Car-gl_3082	-1.01	2.40	249
Car-gl_3144	-0.18	1.98	90

822

823

824

825

826

827

828

829

830

831

832

833

834

835

836

837

838

839

840

841

842

843 **Table 5.** Calibration parameters and mass balance statistics from EISModel applications with four
 844 different datasets of air temperature^a

Temperature dataset	Calibrated parameters		Calibration run (summer 2010)			Validation run (summer 2011)		
	TMF (mm h ⁻¹ °C ⁻¹)	RMF (mm h ⁻¹ W ⁻¹ m ²)	ME (m w.e.)	RMSE (m w.e.)	N&S	ME (m w.e.)	RMSE (m w.e.)	N&S
Measured temperature	0.246	0.00117	-0.027	0.080	0.992	+0.052	0.156	0.888
Standard lapse rate	0.202	0.00100	-0.049	0.252	0.918	-0.160	0.261	0.686
G&B method	0.251	0.00109	-0.006	0.113	0.984	+0.156	0.314	0.545
S&M method	0.291	0.00128	-0.049	0.359	0.832	-0.282	0.366	0.381

	Calibrated parameters		Calibration run (summer 2011)			Validation run (summer 2010)		
	TMF (mm h ⁻¹ °C ⁻¹)	RMF (mm h ⁻¹ W ⁻¹ m ²)	ME (m w.e.)	RMSE (m w.e.)	N&S	ME (m w.e.)	RMSE (m w.e.)	N&S
Measured temperature	0.246	0.00138	+0.006	0.152	0.893	-0.095	0.119	0.982
Standard lapse rate	0.175	0.00111	-0.008	0.210	0.796	+0.178	0.346	0.844
G&B method	0.265	0.00141	+0.045	0.288	0.618	-0.172	0.226	0.934
S&M method	0.236	0.00129	-0.018	0.241	0.732	+0.315	0.522	0.647

845 ^aCalibration in 2010 and validation in 2011 in the upper table, vice versa in the lower table.
 846 Measured vs. modeled values are displayed in Fig. 10.

847

848

849

850

851

852

853

854

855

856

857

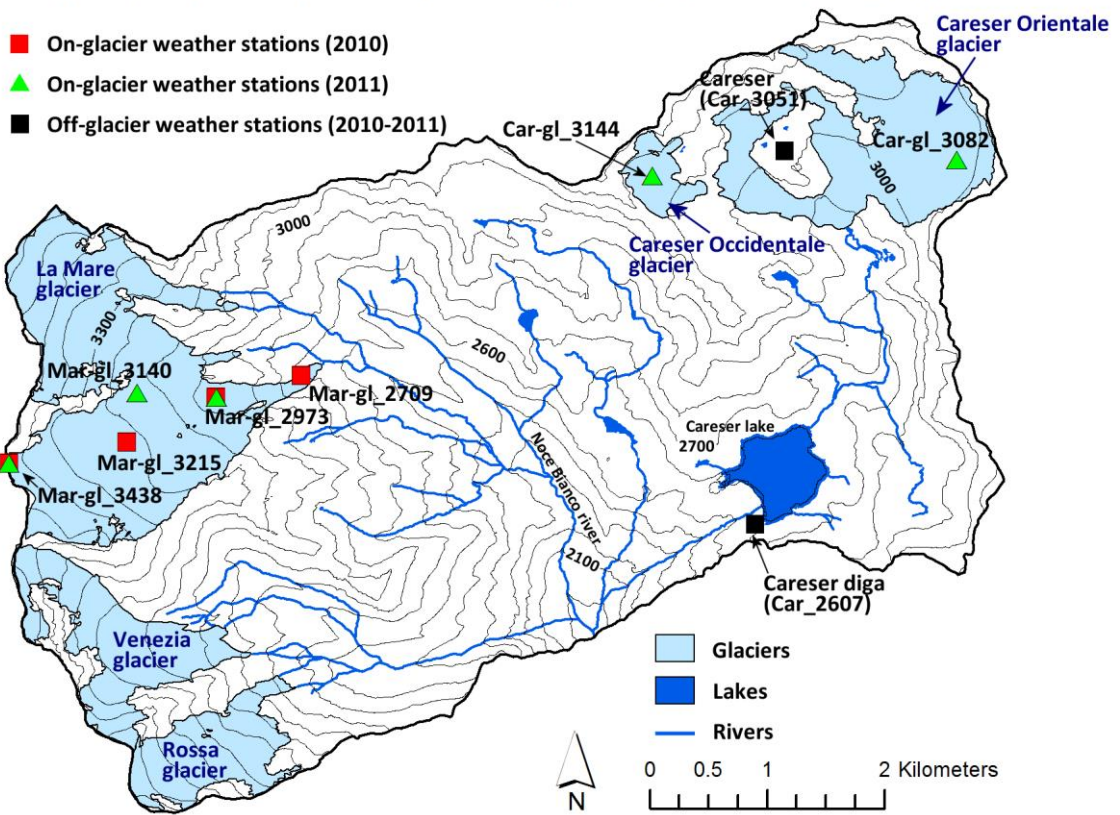
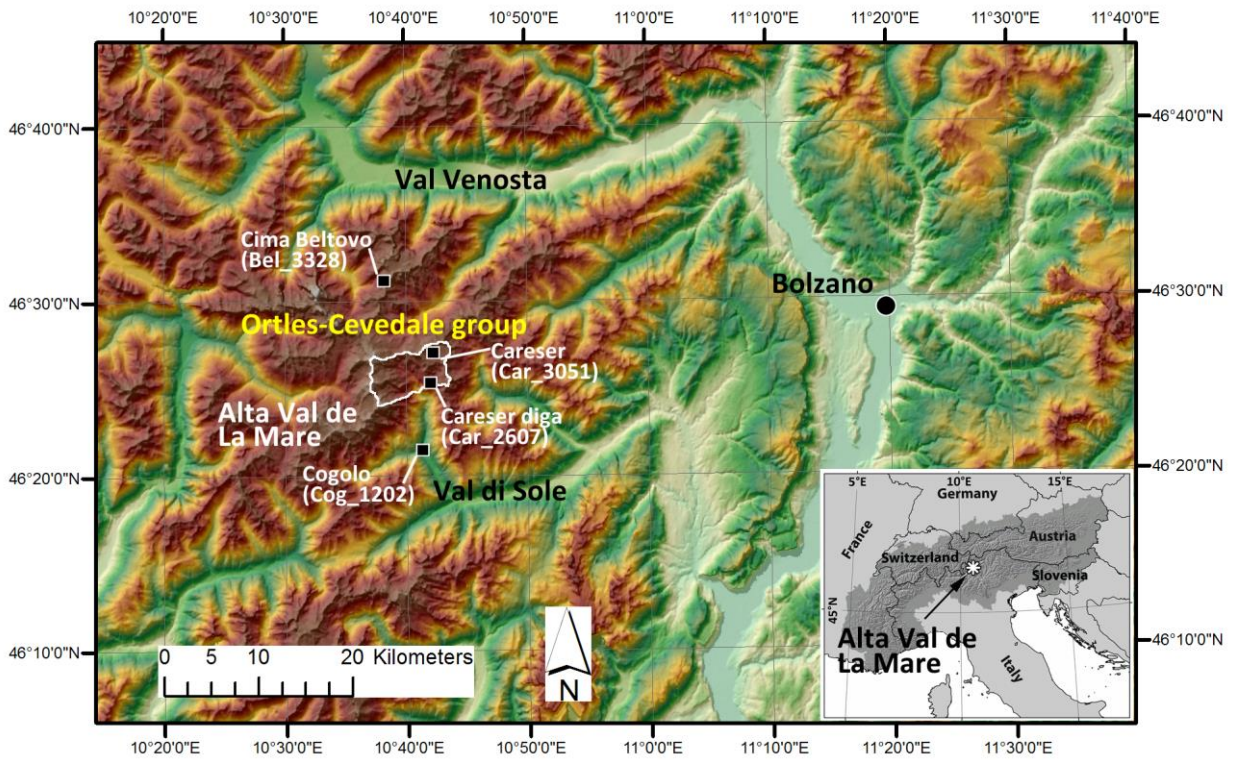
858

859

860

Figures

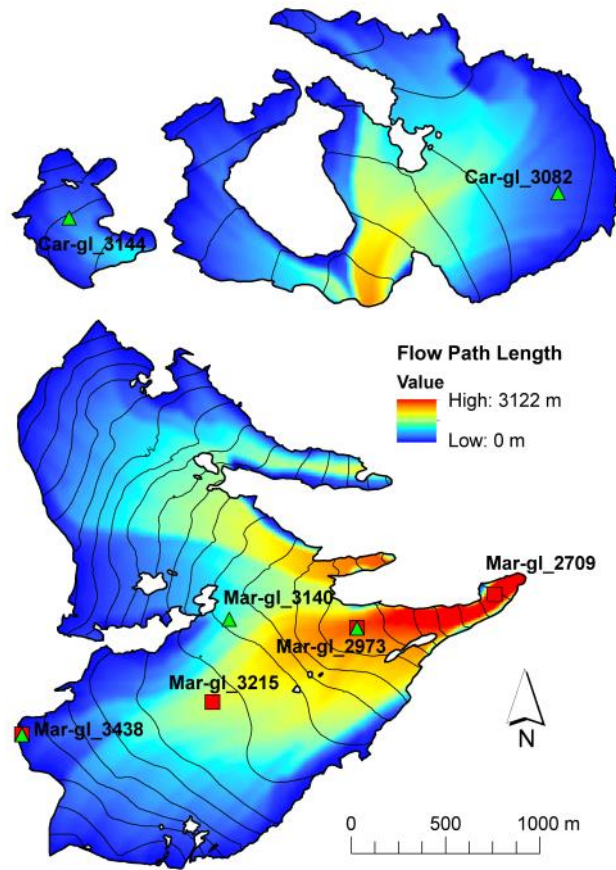
861



862

863 Figure 1 - Geographic setting of Alta Val de La Mare and location of the automatic weather stations.

864



866

867

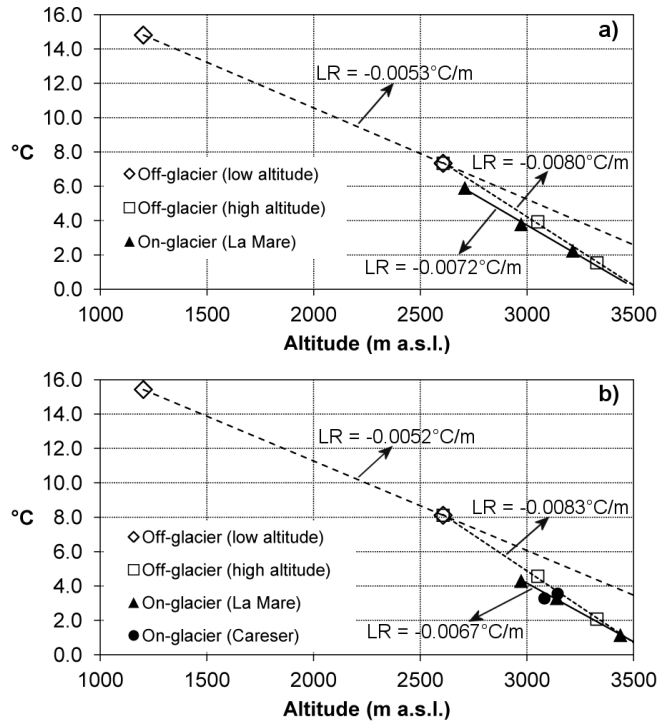
Figure 2 – Map of the flow path length calculated for Careser and La Mare glaciers.

868

869

870

871



872

873 Figure 3 - Mean temperature vs. altitude: a) from 3 July to 23 September, 2010, and b) from 7 July
 874 to 12 September, 2011. Lines indicate linear regressions of temperature vs. altitude for subsets of
 875 weather stations. LR = vertical lapse rates.

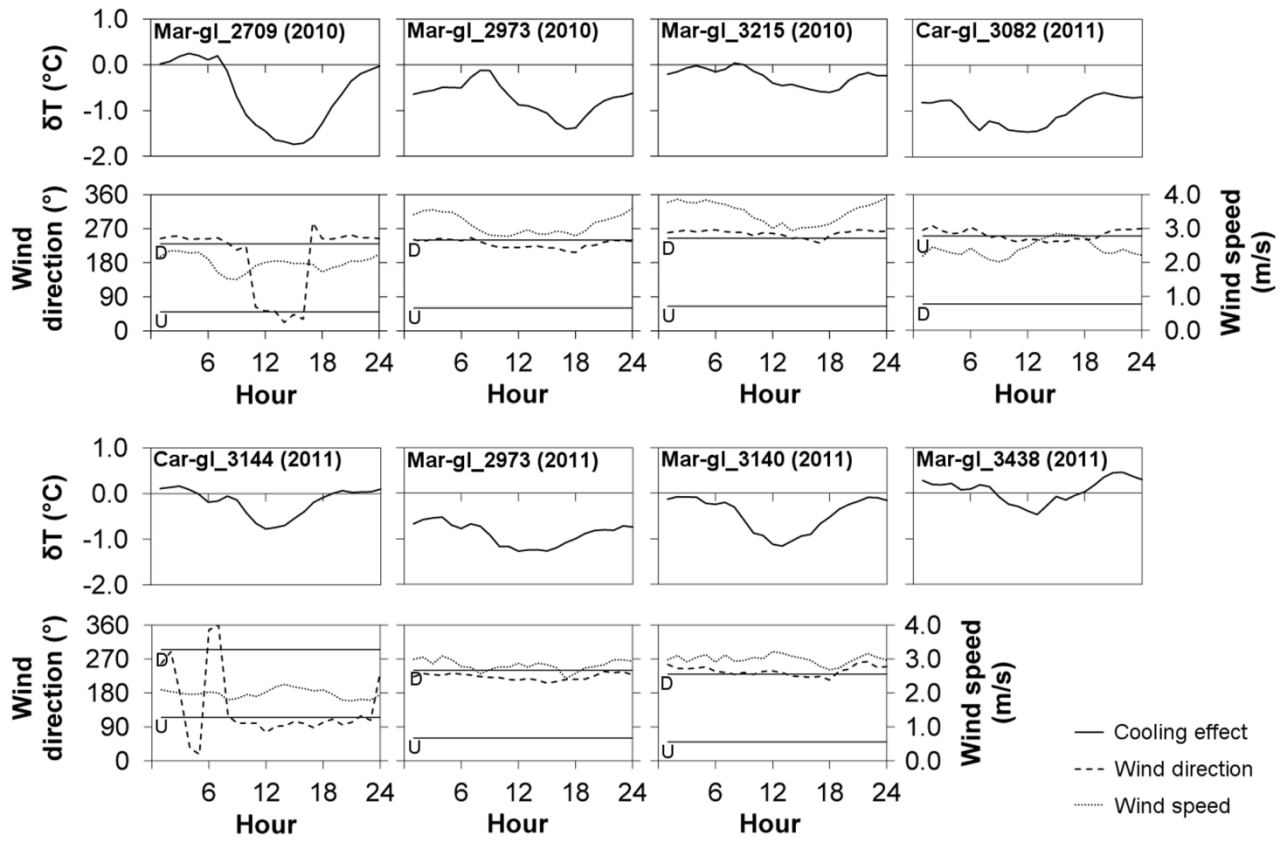
876

877

878

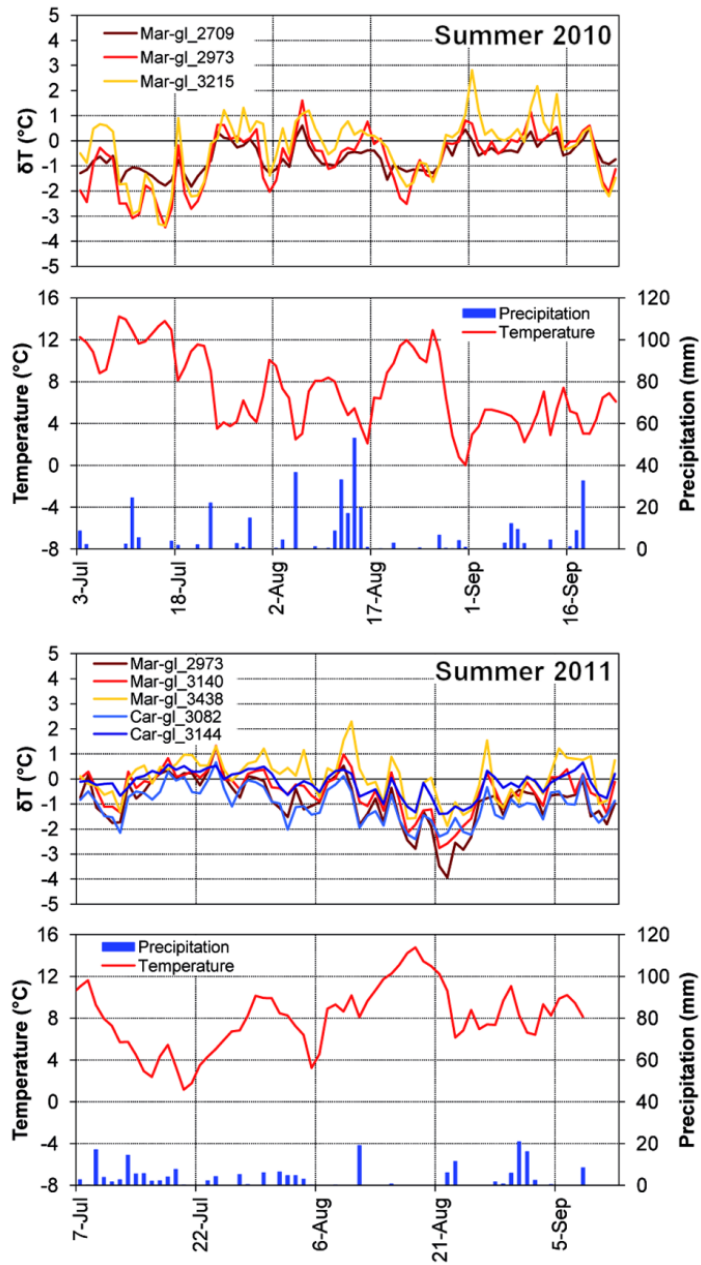
879

880



881

882 Figure 4 - Mean daily cycle of the glacier cooling effect (δT), wind direction and wind speed at the
 883 eight on-glacier weather stations. The operation period of each station is indicated in brackets.
 884 Down-glacier and up-glacier wind directions are indicated with straight lines marked with 'D' and
 885 'U'. Mar-gl_3438 lacks wind data because of anemometer failure.



886

887 Figure 5 - Mean daily cooling effect at the on-glacier weather stations, and corresponding daily
 888 precipitation and mean temperature at Careser diga (Car_2607).

889

890

891

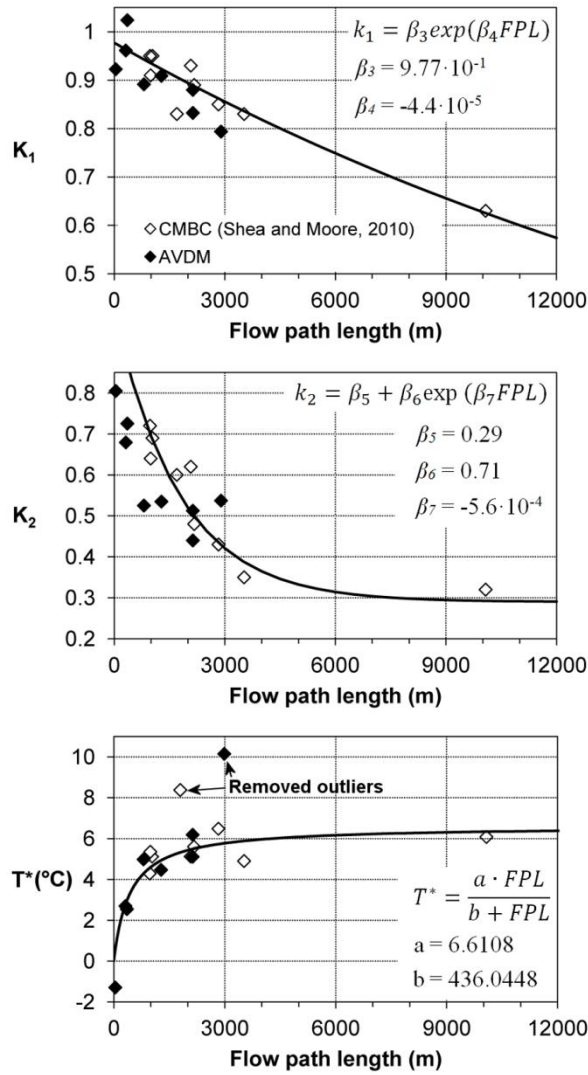
892

893

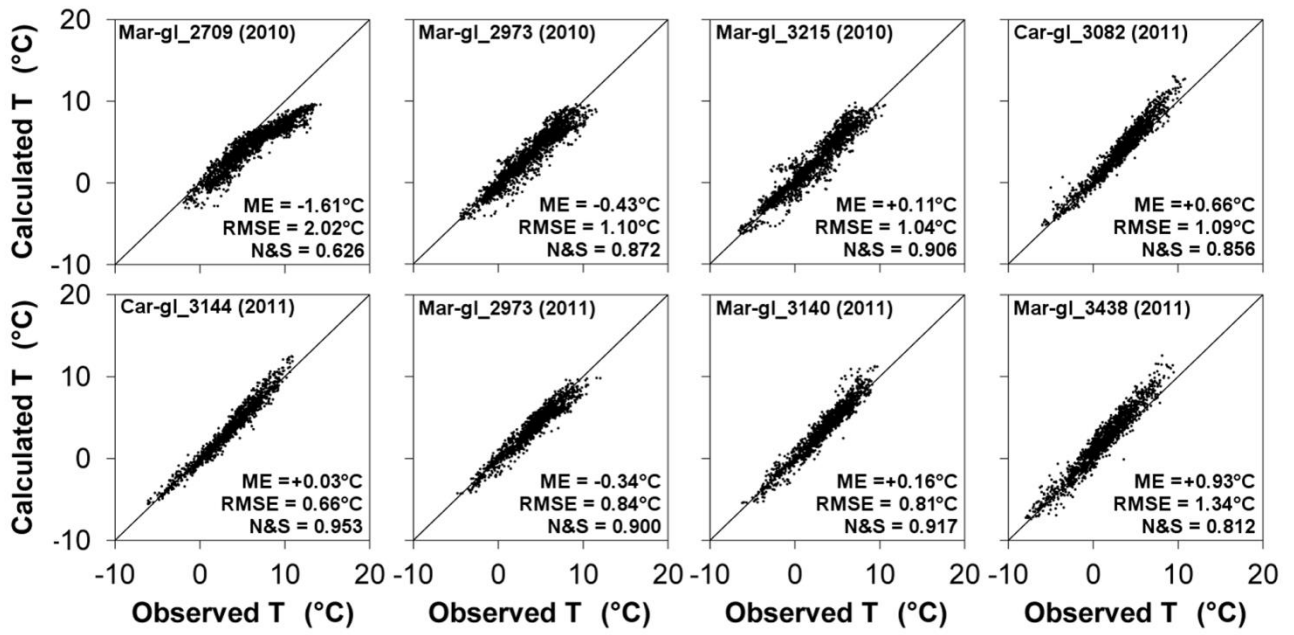
894

895

896



899 Figure 6 - Transfer functions for the coefficients K_1 , K_2 and T^* of the Shea and Moore (2010)
 900 method. CMBC = S&M study area; AVDM = our study area. Outliers due to under-sampling at
 901 freezing temperatures have been removed (as in the S&M work). β_3 to β_7 are coefficients from
 902 S&M (J. M. Shea, personal communication), while the transfer function and coefficients for T^* are
 903 new results from the present work.



904

905 Figure 7 - On-glacier temperature calculated with the Shea and Moore (2010) method vs. observed
 906 temperature.

907

908

909

910

911

912

913

914

915

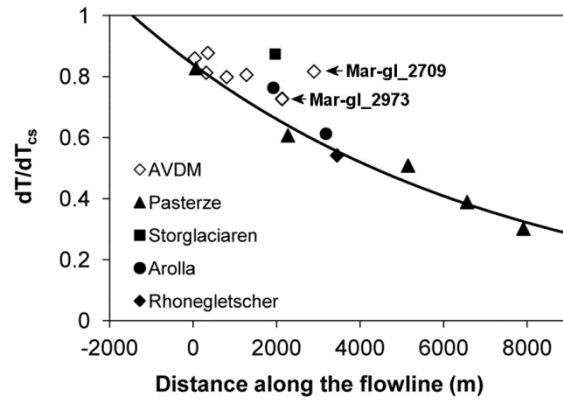
916

917

918

919

920



921

922 Figure 8 - Sensitivity of on-glacier temperature to temperature outside the thermal influence of
 923 glaciers and best fit of Eq. (13) to Pasterze data. Redrawn figure from Greuell and Böhm (1998).
 924 Values measured on Careser and La Mare glaciers (AVDM) have been added for comparison. Mar-
 925 gl_2973: two overlapping points (summer 2010 and 2011 have identical sensitivity).

926

927

928

929

930

931

932

933

934

935

936

937

938

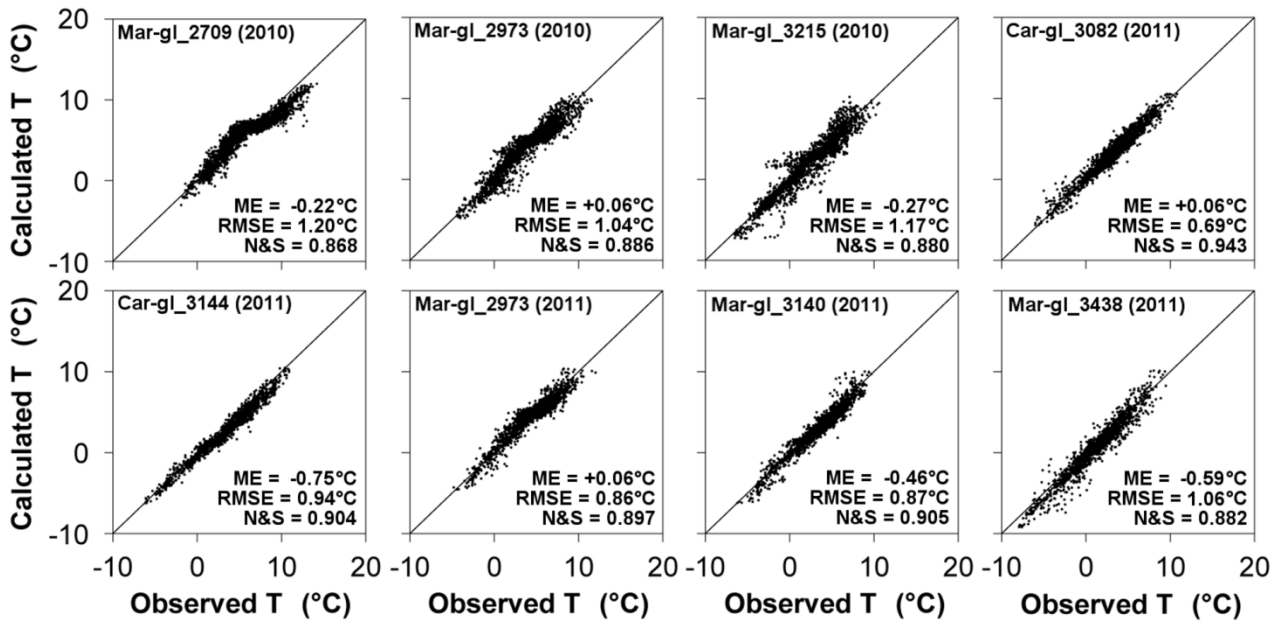
939

940

941

942

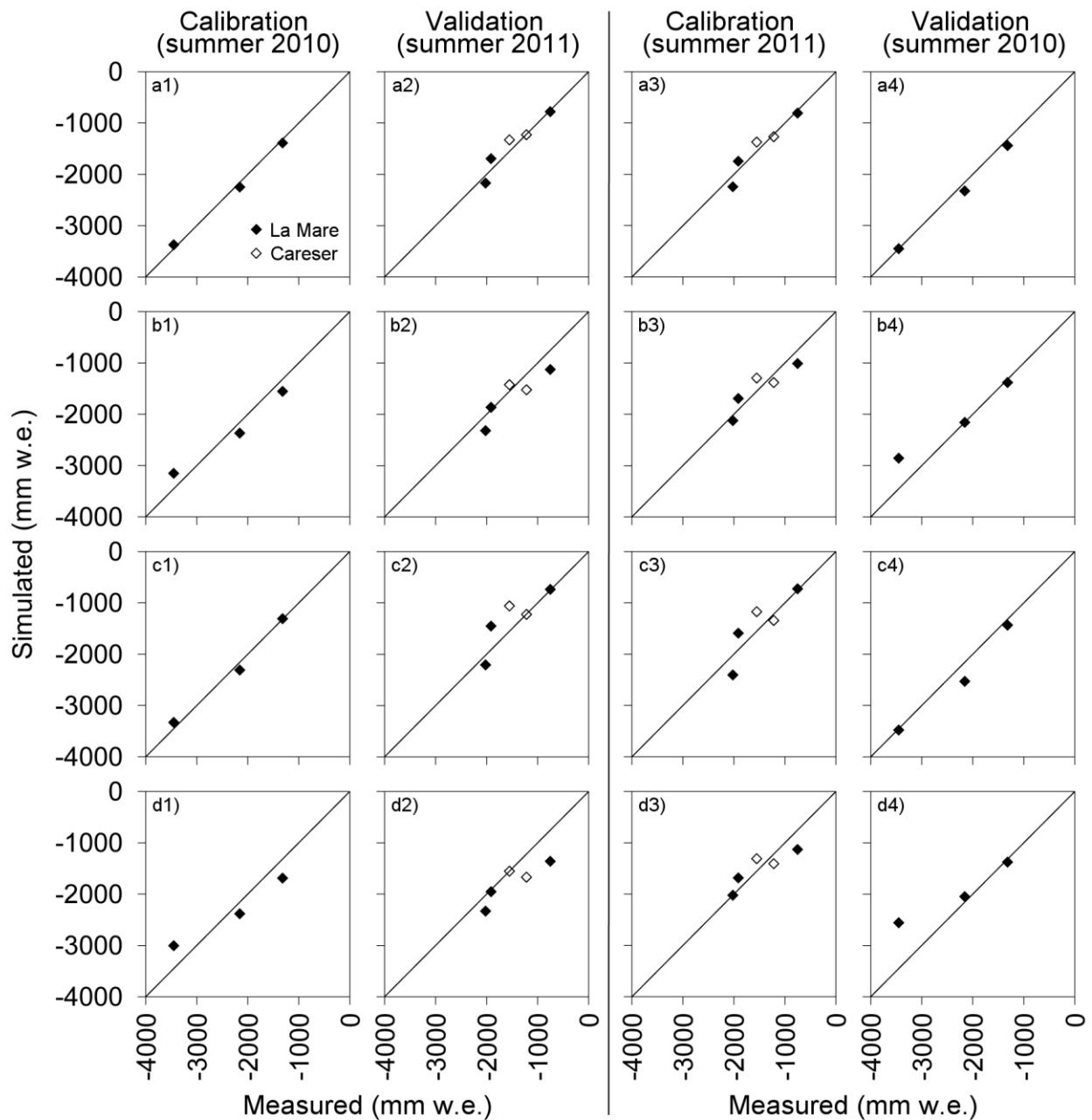
943



944

945

Figure 9 - On-glacier temperature calculated with the G&B method vs. observed temperature.



946

947 Figure 10 - Measured vs. modeled mass balance at the eight glacial weather stations, using
 948 EISModel with four different air temperature inputs: a1 to a4 = measured; b1 to b4 = extrapolated
 949 from Car_2607 via the standard lapse rate ($-6.5^{\circ}\text{C km}^{-1}$); c1 to c4 = calculated via the G&B method;
 950 d1 to d4 = calculated via the S&M method. Corresponding statistics are reported in Table 6.